Atmospheric Research 171 (2016) 107–120

Contents lists available at ScienceDirect

Atmospheric Research

journal homepage: www.elsevier.com/locate/atmosres

Observational and numerical study of the Vardaris wind regime in northern Greece

I. Koletsis *, T.M. Giannaros, K. Lagouvardos, V. Kotroni

National Observatory of Athens, Institute for Environmental Research and Sustainable Development, Vas. Pavlou & I. Metaxa, 15236 Athens, Greece

ARTICLE INFO

Article history:
Received 14 October 2015
Received in revised form 18 December 2015
Accepted 18 December 2015
Available online 29 December 2015

Keywords:
Wind channeling
Gap flow
Complex topography
Vardaris
WRF
Greece

ABSTRACT

The Axios Valley, located in central-northern Greece, is surrounded by complex topography that plays a significant role in the modification of wind flow, both in terms of speed and direction. The characteristic wind regime of this valley is Vardaris, a northwesterly wind that prevails in this region, especially during the cold period of the year. Vardaris is well known for its consistent direction and high intensity, as well as for the effective advection of cold and dry air, often resulting to significant damages in local infrastructures and agriculture. A field campaign under the name AXIOS took place during the period from November 2007 through May 2008 in order to examine this particular wind flow. The analysis of the in situ observational data, which was funded by the research program THESPIA-KRIPIS, showed that topography plays a key role in intensifying Vardaris, generating gusts that approximated 30 m s^{-1} during the experimental period. The air temperature and humidity fields were also found to be significantly influenced. In addition to the observational study, an intense Vardaris episode was simulated with the Weather Research and Forecasting (WRF) model at high horizontal resolution. Results revealed that the model was able to reproduce the favorable environmental conditions that lead to Vardaris occurrence, providing a useful insight on the physical mechanisms explaining its structure.

1. Introduction

Topography is documented as a well-known parameter generating thermally and dynamically driven wind flows (Whiteman and Doran, 1993; Steenburgh et al., 1998; Mayr et al., 2007; Koletsis et al., 2010; Shimada et al., 2012; Lennard, 2014). Gap flows and wind channeling, in particular, are two widely recognized manifestations of wind flow modification due to topography. Wind channeling refers to the phenomenon of wind inside a valley blowing along the valley's axis (Weber and Kaufmann, 1998; Kossmann and Sturman, 2003; Carrera et al., 2009; Deacu et al., 2010). This phenomenon has been reported in several regions around the world, including the St. Lawrence River Valley in Canada (Carrera et al., 2009), the Tennessee Valley in the United States (Eckman, 1998), the mountainous area near Basel in Switzerland (Weber and Kaufmann, 1998), the Kongsfjorden–Kongsvegen Valley in Norway (Esau and Repina, 2012), the upper Rio Negro Valley in Argentina (Cogliati and Mazzeo, 2006), and the upper Rhine Valley in Germany (Gross and Wippermann, 1987). The physical mechanisms that are responsible for the generation of channeled winds are presented in the early work of Whiteman and Doran (1993), also discussed in the more recent study of Carrera et al. (2009). Briefly, these mechanisms are the thermally driven channeling, downward momentum transport, forced channeling, and pressure-induced channeling.

The definition of gap flow or gap wind dates back to the beginning of the 1930s (Reed, 1931). Simply put, this term is used to describe the flow of wind between indentations in orography, resulting either from purely horizontal topographical constrictions (level gaps) or from both horizontal and vertical constrictions, such as mountain passes (Mayr et al., 2007). Gap winds develop primarily due to the pressure gradient existing in the along-gap direction (Colle and Mass, 1998; Steenburgh et al., 1998; Mayr et al., 2007). The presence of these winds has been reported in several areas around the globe, including the Strait of Juan de Fuca (Colle and Mass, 2000) and the Columbia Gorge (Sharp and Mass, 2004) in the United States, the Cook Strait in New Zealand (Reid, 1996), the Gulf of Tehuantepec in Mexico (Steenburgh et al., 1998) and the Shelikof Strait in Alaska (Lackmann and Overland, 1989). In the majority of these studies, maximum wind speeds were reported well downstream of the narrowest constriction, at the end of the gap exit, contrary to the Venturi effect, which is often used as an explanation for the occurrence of strong gap winds (Reed, 1931). A comprehensive review of the knowledge acquainted for gap flows through the Mesoscale Alpine Programme is available in Mayr et al. (2007).

The Axios Valley is a major topographical feature of central-northern Greece (Fig. 1a). It owes its name to the Axios River that flows from FYROM through Greece and into the Thermaikos Gulf (Fig. 1b). The fairly high mountains and hills that surround the valley play a significant role in the modification of wind flow. Indeed, the Axios Valley has

* Corresponding author. Tel.: +30 2108109134.
E-mail address: koletsis@noa.gr (I. Koletsis).

http://dx.doi.org/10.1016/j.atmosres.2015.12.011
0169-8095/

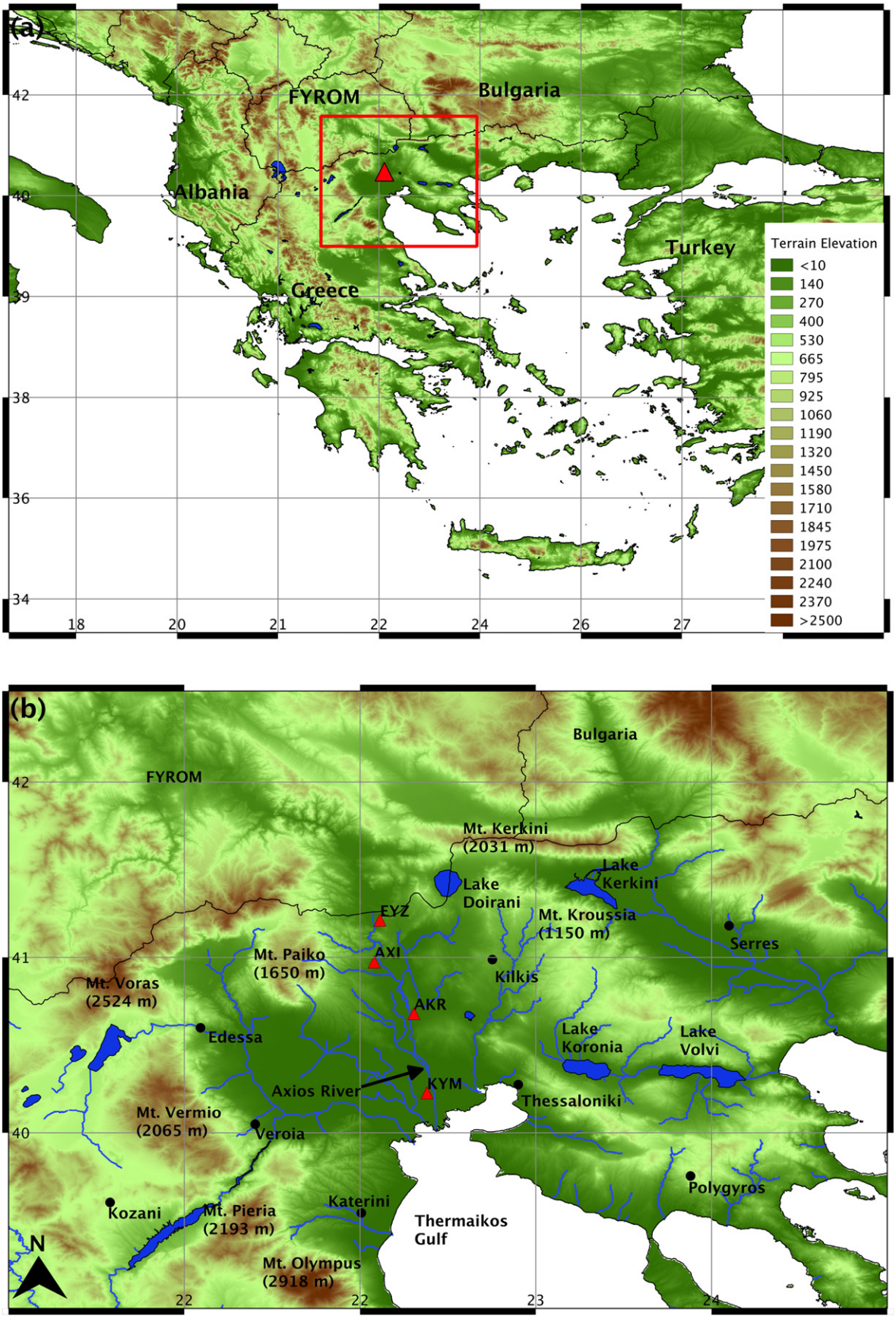

Fig. 1. (a) Topographic view of Greece and neighboring countries with identification of the greater study area (red box) and Axios Valley (red triangle). (b) Topographic view of the greater study area with identification of major topographic elements. Black circles and red triangles denote the location of major cities and measurement sites, respectively. The legend for elevation is common to both maps.

been well known to meteorologists in Greece due to a northwesterly wind, called Vardaris ("Vardar" is the Serbian name for Axios River) prevailing in the region under certain synoptic-scale setups. This particular wind blows along the central ridge of Mt. Paiko and Mt. Kerkini (Fig. 1b) and is more prominent during the cold period of the year. Vardaris is primarily characterized by its consistent direction and high intensity, and the effective advection of cold and dry air. Intense episodes of this local wind often result to significant destructions in infrastructures and agriculture. Further, the wind flow that characterizes Vardaris is considered to be one key factor for the occurrence of snowfall in the major coastal city of Thessaloniki (Fig. 1b) (Giannoulakis, 2014).

Despite its peculiar and often devastating characteristics, the availability of studies focusing on Vardaris is extremely restricted (Angouridakis et al., 1981; Maheras et al., 1984; Psarri, 2005; Tsopouridis et al., 2013). Considering this research gap, the National Observatory of Athens (NOA) designed a field campaign, namely AXIOS, which was carried out with the support of the Department of Meteorology and Climatology (DMC) of the Aristotle University of Thessaloniki (AUTH), with the aim to examine the particular wind regime of Vardaris. Recently, Tsopouridis et al. (2013) utilized a small portion of the AXIOS dataset to provide a preliminary study of Vardaris following a purely numerical modeling approach.

Considering the above-described context, the purpose of this work is twofold. First, it exploits the full dataset of the AXIOS campaign in order to provide a comprehensive observational study of Vardaris during the 7-month experimental period; second, this study employs a state-of-the-art numerical weather prediction (NWP) model, namely the Weather Research and Forecasting (WRF), to examine the characteristics of an intense Vardaris episode and the physical mechanisms responsible for its development. Employment of mesoscale models, such as WRF, has already provided a significant enhancement to both the understanding and predictability of mountain waves and downslope wind events (e.g. Czyzyk and Bell, 2007). In particular, the WRF model has been used in several past studies for examining wind regimes over complex terrain (Papanastasiou et al., 2010; Miglietta et al., 2013; Puliafito et al., 2015) and windstorms driven by synoptic patterns (Simon et al., 2011), as well as for evaluating the influence of land-state representation on the reliability of wind simulations (Santos-Alamillos et al., 2015) or even for producing historical wind databases (Manor and Berkovic, 2015). In essence, the present work should be considered to be an important contribution to the understanding of the significant local wind regime of Vardaris.

2. Data and methodology

Two different sources of data were employed for conducting the present study. Observational data, provided by ground-based weather stations, were used for examining the wind regime of the Axios Valley during a 7-month period. Numerical modeling data were then used for the analysis of an intense episode of the Vardaris wind.

2.1. Observational data

The observational data used in this study were derived from four automatic meteorological stations deployed along the Axios Valley during the period from November 2007 to May 2008. The locations of the stations are shown in Fig. 1b, while Table 1 summarizes key information about the measurement sites. Two stations were installed at the two edges of the valley into the Greek territory, namely Eyzonoi and Kymina. The other two stations, namely Axioupoli and Akropotamos, were deployed within the valley and nearby the banks of Axios River. Each station was equipped with a three-cup anemometer and vane, a rain gauge, a temperature and humidity sensor, protected by a fan-aspirated radiation shield, and a barometer. Wind and temperature/humidity were measured at 10 m and 2 m above ground level, respectively. The stations' data sampling was 2.5 s, while for the statistical analysis, data averaged over 5 min were used. It is worth noticing that all stations were situated in rural locations in order to avoid any urban-induced effects on measurements.

Table 1
List of stations and summary of characteristics of the measurement sites used in the context of AXIOS campaign.

Station	Code	Latitude (°N)	Longitude (°E)	Elevation (m asl[a])
Eyzonoi	EYZ	41.1068	22.5464	58
Axioupoli	AXI	40.9808	22.5516	33
Akropotamos	AKR	40.8402	22.6576	44
Kymina	KYM	40.6199	22.6999	2

[a] asl: above sea level.

2.2. Numerical modeling data

The NWP model used in this study is WRF, version 3.6.1 (Skamarock et al., 2008), a next-generation mesocale numerical weather prediction system designed to serve both operational forecasting and atmospheric research needs (Borge et al., 2008; Challa et al., 2009). Three 1-way nested modeling domains with horizontal grid resolution of 20 km (mesh size of 215 × 205), 5 km (mesh size of 133 × 121), and 1 km (mesh size of 236 × 256) were defined for carrying out the numerical simulation, of which the innermost high-resolution domain focused on the study area (Fig. 1a). In the vertical, 50 unevenly spaced sigma levels were specified with the model top defined at 100 hPa, to allow for a detailed representation of the vertical structure of the atmosphere under the influence of Vardaris. Approximately 20 levels were placed in the lowest 1 km of the model.

Radiation (shortwave and longwave) was parameterized with the updated Rapid Radiative Transfer Model (RRTMG) scheme (Iacono et al., 2008) and the Thompson parameterization (Thompson et al., 2008) was used for microphysics processes. The Mellor–Yamada–Janjic scheme (Janjic, 1994) was employed for the parameterization of the planetary boundary layer, while land-surface processes were parameterized with the unified Noah land surface model (Tewari et al., 2004). The Kain–Fritsch convection parameterization scheme (Kain, 2004) was used for the outermost modeling domain, while for the two inner domains, convection was resolved explicitly.

SRTM (Shuttle Radar Topography Mission) data, resampled to 250 m grid spacing (Jarvis et al., 2008), were used for the representation of topography in the highest-resolution modeling domain. For the other two domains, the standard USGS (United States Geological Survey) topography dataset was employed (at 2-arc-min resolution for the outermost domain and at 30-arc-sec resolution for the second-level domain). Default 20-category MODIS-based (Moderate Resolution Spectroradiometer) data at 30-arc-sec resolution were used for the parameterization of land use in all modeling domains.

WRF was implemented for simulating an intense Vardaris episode that occurred on 10 November 2007. The numerical simulation was initialized on 9 November 2007 at 1800UTC and extended to 30 h, allowing for a 6 h model spin-up period. Although this model spin-up period is considered to be rather short, it was found that it allowed for better resolving the synoptic setup and consequently the initialization and evolution of the examined episode, compared to larger spin-up periods. For the initialization of the model, the 0.25° × 0.25° spatial resolution and 6 h temporal resolution operational atmospheric analysis surface and upper-air data of ECMWF (European Centre for Medium-Range Weather Forecasts) were used. WRF outputs were archived at 5 min intervals.

3. Data analysis for the AXIOS experimental campaign

This section presents the wind regime, as well as the relationship between the wind, and the temperature and humidity fields along the Axios Valley during the 203 days of the experimental period (i.e. November 2007 to May 2008).

3.1. Wind data analysis

The distribution of the wind direction during the experimental period for the ground stations is presented in Fig. 2a. The northwestern sector winds (from west-northwestern to north directions) prevail at all ground stations; with the north-northwestern direction at AXI station presenting the largest frequency percentage, ~32%, followed by AKR station (~23%). At EYZ, which is the northernmost station, the northern winds dominate, while the northwesterly winds also prevail at the southernmost ground station of KYM, with frequencies of occurrence of 21% and 18%, respectively. Further, it is evident that the north and north-northwestern winds are also those with the strongest intensities (Fig. 2b).

The observed winds were classified in six categories: the calm class with zero mean wind speed, the light wind class (1–3 m s^{-1}), the near moderate class (4–7 m s^{-1}), the moderate class (8–10 m s^{-1}), the strong class (11–13 m s^{-1}), and the near gale class with mean wind speeds greater than 14 m s^{-1}. For all measurement sites, the maximum frequency of occurrence is observed at the light class category, followed by the calm category for the northern stations of EYZ and AXI and the near moderate for AKR and KYM stations (Fig. 2c). The maximum frequency of occurrence of the strong as well as of the near gale winds is observed at EYZ station. The distribution of wind direction for the near gale wind class (≥14 m s^{-1}) reveals that the north-northwesterly winds are the most frequent (55%–85%) for all considered locations (EYZ, AKR, KYM), except from AXI where northwesterly winds prevail with a percentage of ~70% (Fig. 2d). Moreover, the investigation of the diurnal variability of the near gale class revealed that the higher wind speeds are observed during the morning and early noon hours presenting the maximum percentage of occurrence between 0900 UTC to 1400 UTC (not shown).

The strongest winds observed under the northwestern sector regime are related to fluctuations in the wind speed at periods as short as a few seconds. These fluctuations, known as wind gusts, can cause damages in constructions and problems in road traffic, as their strength may exceed twice the mean wind speed (Durran, 1990). During the study period, the maximum wind gusts were recorded at EYZ and KYM, approaching 29 m s^{-1} and 28 m s^{-1}, respectively. The strength of the wind gusts is described by the gust factor, which is calculated from the ratio of peak gust to the sustained speed (Agustsson and Olafsson, 2004). The sustained wind speed is the mean wind speed over a 5-min averaging period, while the peak gust is the highest value recorded during this time interval. In this study, gust factors were calculated for mean wind speeds greater than 5 m s^{-1}.

The higher values of mean gust factor were computed at AXI (1.52) and EYZ (1.39) stations. On the other hand, the lowest values were calculated at KYM (1.37) and AKR (1.33) sites. Fig. 3 presents the box-and-whisker diagram of the gust factor at the AXI station, in which the highest gust factor was calculated. The graph shows a slightly decreasing wind gust factor with increasing mean wind speed. A possible explanation for the high values of gust factor at AXI and EYZ is the surrounding complex topography, and primarily the adjacent high mountains located west-northwest of these stations (Fig.1b). This finding is in agreement with Agustsson and Olafsson (2004), who showed that the gust factor is strongly related to the distance and the dimensions of the adjacent mountains, producing strong gusts downstream.

3.2. Temperature and humidity data analysis

The majority of the studies devoted to the interaction of the wind flow with topography underline that the terrain-induced wind flow could also be responsible for the modification of the temperature and humidity fields (e.g. Sharp and Mass, 2004; Koletsis et al., 2009b). In order to investigate the relationship between the northwesterly wind flow and the temperature and humidity, data for each station were analyzed for all wind directions but also for northwestern sector only (northwest, north-northwest, and north wind direction). In order to exclude from the analysis the low temperatures due to surface temperature inversions, the mean temperature and humidity values were calculated only when the mean wind speed exceeded 5 m s^{-1}. The entire analysis was carried out separately for the winter (January, February, and December) and the transitional (March, April, May, and November) months of the experimental period (Fig. 4).

Results reveal that the temperature and humidity fields are strongly influenced by the wind direction. Winter mean temperatures are lower by about 1–5 °C when the wind blew from the northwestern sector, with the largest difference observed at EYZ, and the lowest at KYM (Fig. 4a). The mean temperature during the transition months presents a quite similar behavior; however, the mean temperature difference between categories was obviously smaller (Fig. 4b). The humidity field

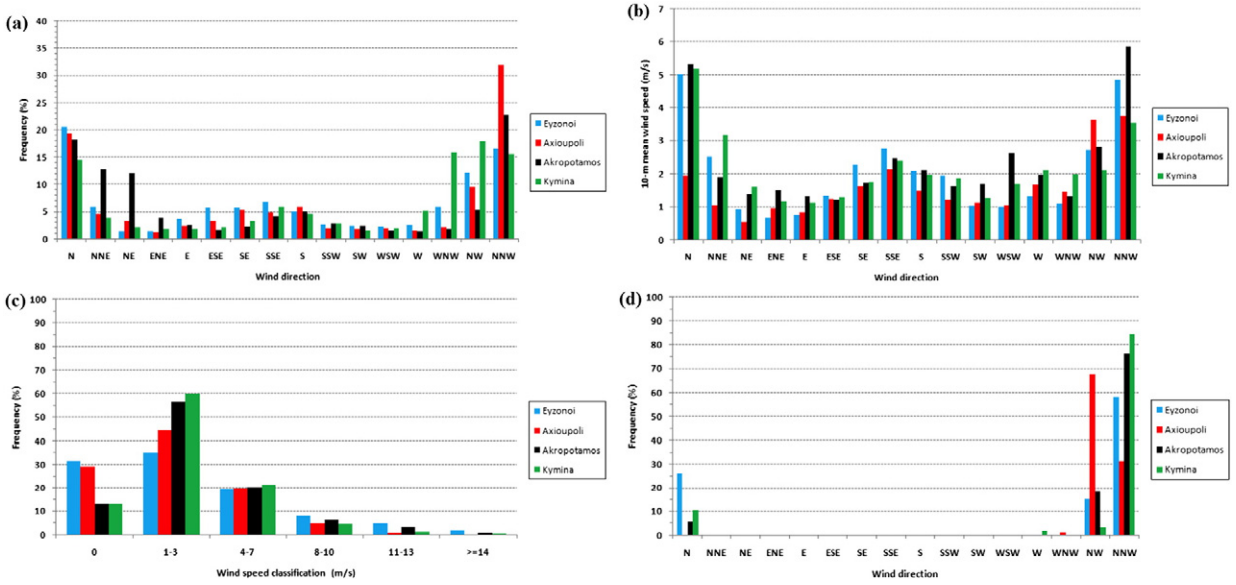

Fig. 2. Bar diagrams for all measurement sites, for (a) frequency of occurrence (%) as a function of wind direction, (b) wind speed distribution per wind direction, (c) frequency of occurrence (%) as a function of the wind speed class, and (d) frequency of occurrence (%) as a function of wind direction for the near gale wind class.

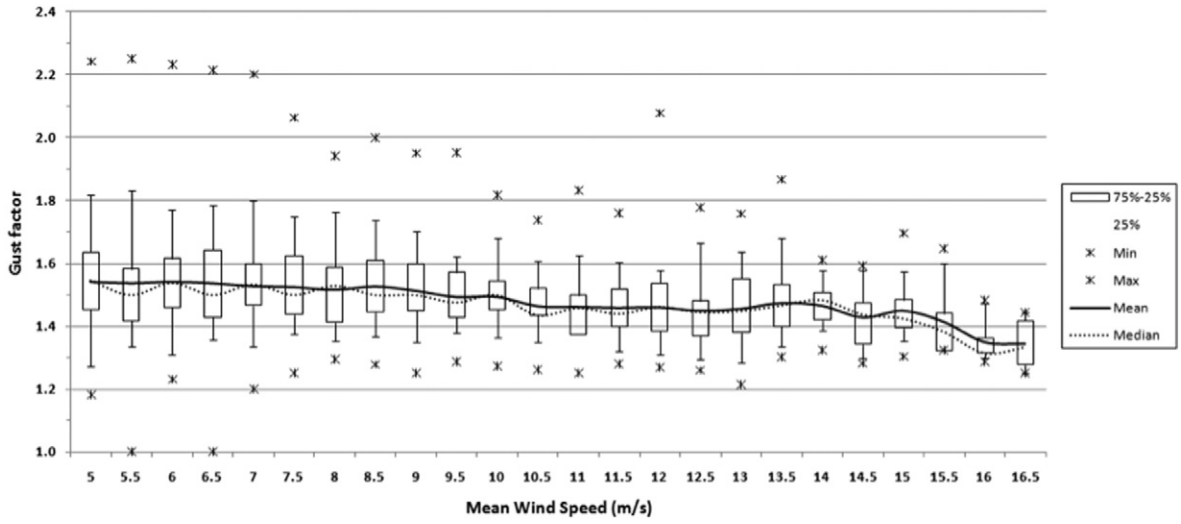

Fig. 3. Boxplot (box-and-whisker diagram) for Axioupoli station (AXI). The upper edge of the box indicates the 75th percentile of the data set, and the lower edge indicates the 25th percentile. The ends of the vertical lines indicate the 5th and 95th percentile of data values, while the two asterisks represent the maximum and the minimum value, respectively. Also, lines depict the mean value as well as the median (50%) of the data. The lower threshold of 5 m s^{-1} from AXI throughout the experiment period was used.

shows also a clear dependence on wind direction for both periods. The vapor pressure values of the northwestern wind sector are lower by about 2 Pa during the winter months (Fig. 4c), while the vapor pressure difference during the transitional months is reduced to approximately 1 Pa (Fig. 4d). This decrease in vapor pressure for both time periods implies that the northwest winds over these regions are also drier.

3.3. Pressure gradient and wind speed correlation

The pressure gradient along a gap is commonly used for investigating the strength of the gap flow. The pressure difference between the gap entrance and exit implies a good indicator of the gap wind strength as the gap flow is associated with large and complex local scale pressure perturbations that are closely related to topography (Overland and Walter, 1981; Colle and Mass, 2000; Sharp and Mass, 2004; Koletsis et al., 2010). In order to examine a possible relationship between the wind speed at stations downstream of EYZ and the pressure gradient along the valley, wind data for all stations that were characterized by northwestern sector (northwest, north-northwest, and north) winds exceeding 5 m s^{-1} were used. Table 2 presents the correlation of the pressure gradient with wind speed for all combinations of stations. The calculated correlation coefficients are mostly positive but relatively

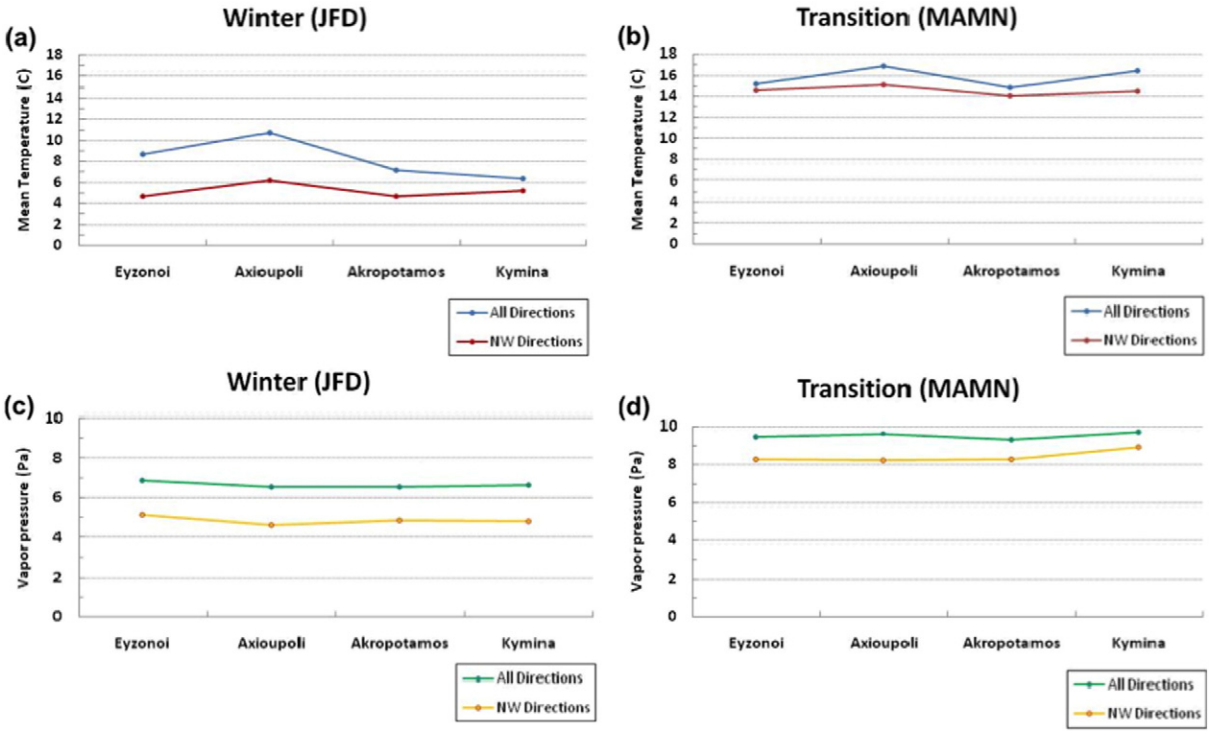

Fig. 4. Mean (a, b) air temperature and (c, d) vapor pressure at 2 m above ground at all measurement sites for (a, c) the winter months and (b, d) the transitional months of the experimental period. The minimum wind speed threshold of 5 m s^{-1} was selected for deriving the mean values. Vapor pressure values were derived from the air temperature and relative humidity temperatures, employing the Goff–Gratsch equation (World Meteorological Organization, 2000).

Table 2
Correlation coefficients between pressure gradients and wind speeds exceeding 5 m s^{-1} under the northwestern wind sector regime.

Pressure difference	AXI	AKR	KYM
EYZ-AXI	0.35	0.30	0.19
EYZ-AKR	0.19	0.22	0.19
EYZ-KYM	0.21	0.20	0.36
AXI-AKR	−0.22	−0.09	0.02
AXI-KYM	−0.11	−0.06	0.33
AKR-KYM	0.09	0.02	0.39

low. The highest correlation coefficients are calculated for the winds observed at the southernmost station of KYM relatively to its pressure difference with its closest station AKR in the southern areas of the valley ($r = 0.39$) but also with the northern stations at AXI ($r = 0.33$) and EYZ ($r = 0.36$). A possible explanation for the low values of correlation coefficient is the fact that the selected stations are located inside the valley and not at the edges; a station located northern of EYZ nearby the gap entrance would give greater values of the correlation coefficient.

4. Numerical simulation of an intense Vardaris episode

Two intense Vardaris episodes took place during the AXIOS campaign, on 10 and 27 November of 2007. Both events were characterized by sustained mean wind speeds exceeding 20 m s^{-1} and gusts approximating 30 m s^{-1}. For the purposes of this study, the event of 10 November 2007 was selected due to the extensive damages induced on infrastructures along the Axios Valley.

4.1. Synoptic-scale setup

The spatiotemporal evolution of the mean sea-level pressure field over Europe on 10 November 2007, as derived from the ECMWF analysis and the 20 km WRF simulation, is summarized in Fig. 5. It is noticeable that the WRF-resolved synoptic-scale atmospheric circulation matches closely the observed setup, although small differences do exist. Indeed, ECMWF and WRF surface analysis data agree in that the examined Vardaris episode developed as a result of the interaction between a low-pressure system crossing southern Balkans and an

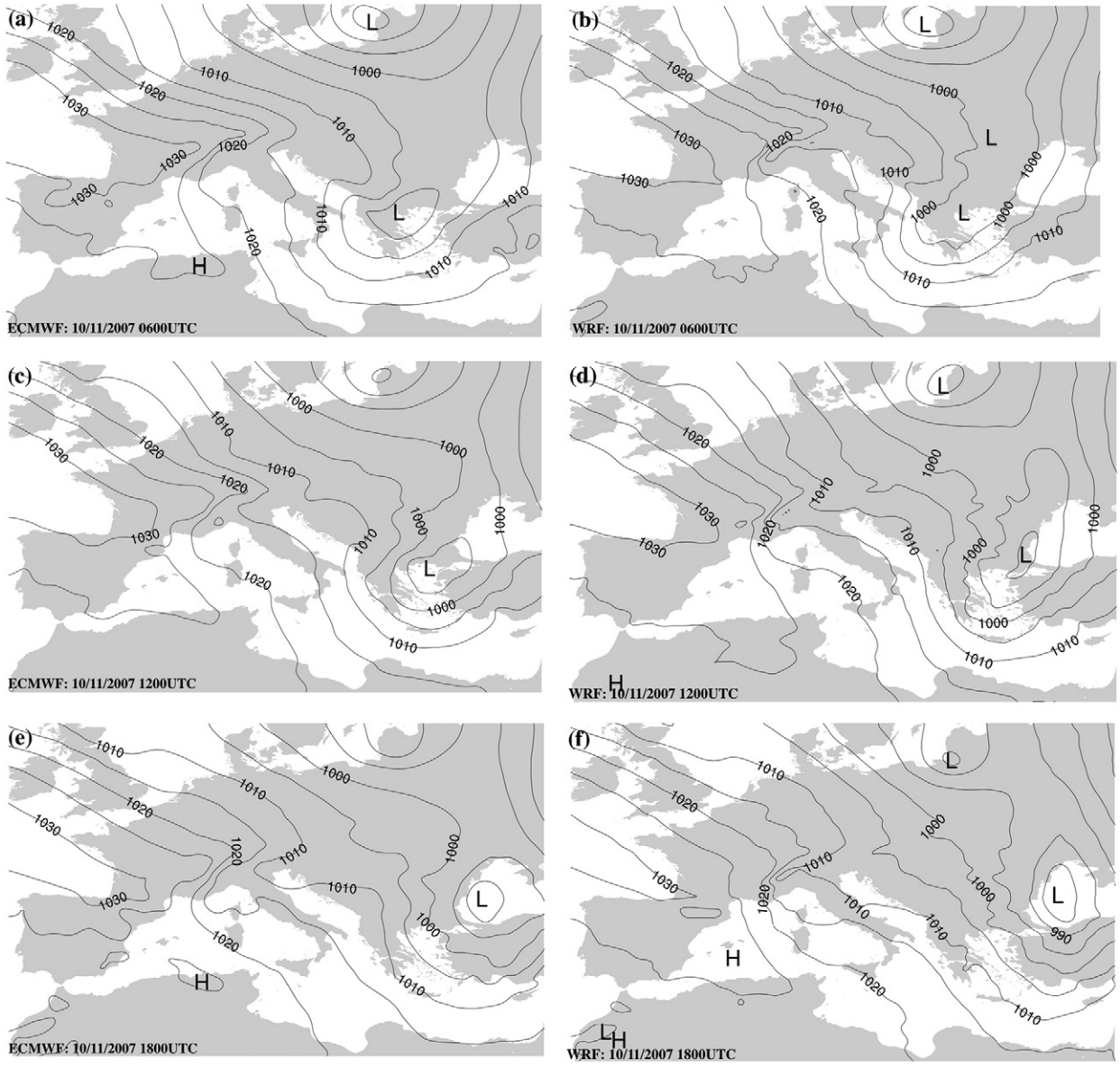

Fig. 5. Mean sea-level pressure (at 5 hPa intervals) derived from 0.25° × 0.25° spatial resolution ECMWF operational atmospheric surface analysis (left column) and 20 km WRF simulation (right column), valid at 10 November 2007 (a, b) 0600 UTC, (c, d) 1200UTC, and (e, f) 1800 UTC.

anticyclone influencing west and central Europe. The resulting pressure gradient led to the establishment of the characteristic northwesterly flow of Vardaris in the study area, coinciding with the passage of the depression's trailing cold front (not shown). However, it is clear that in the WRF simulation, the trespassing depression deepens and moves slightly faster than in the ECMWF analysis. In essence, this is expected to have an impact on the numerically resolved evolution of the episode, as it will be later discussed (Section 4.2).

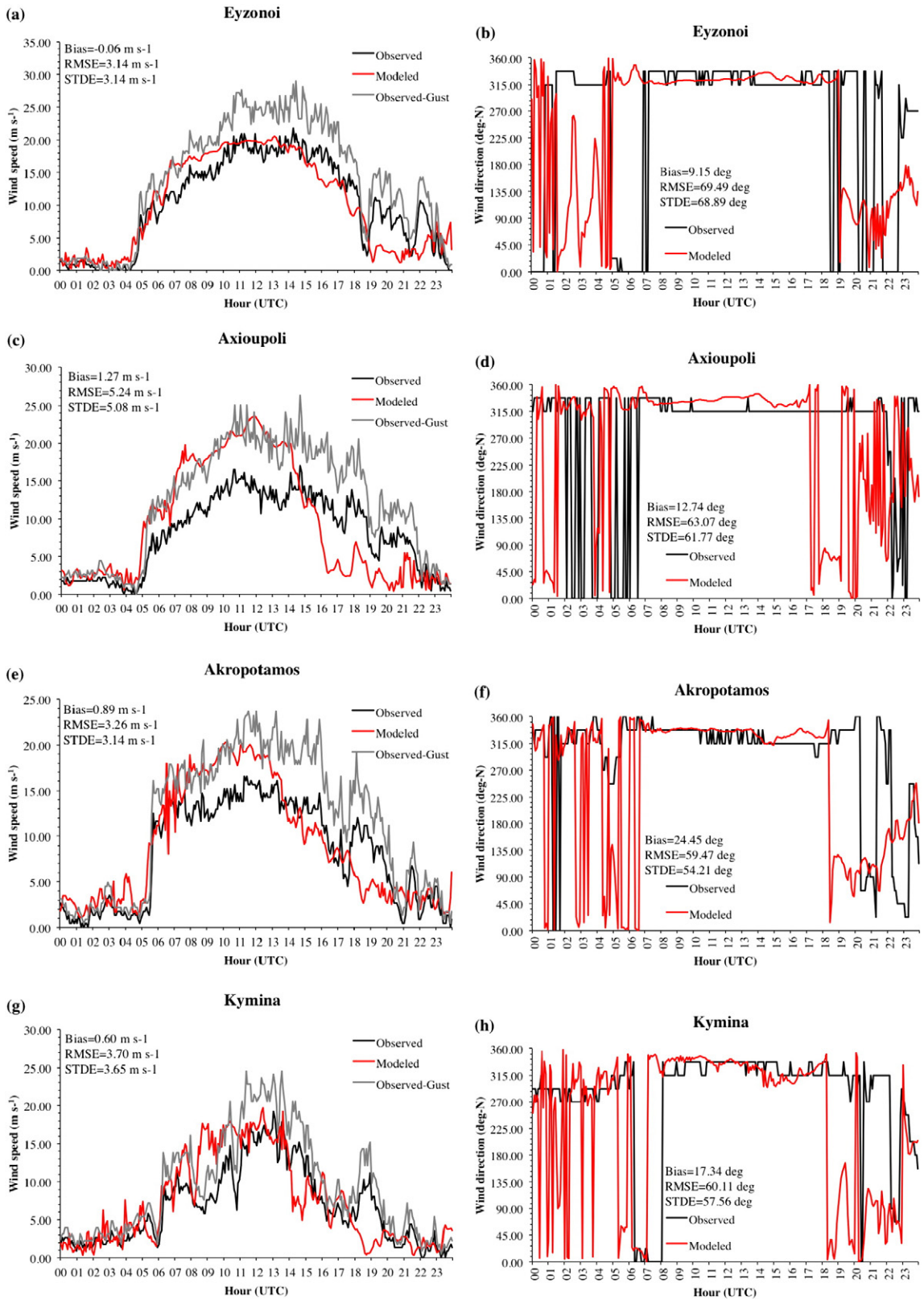

Fig. 6. Times series of observed and modeled wind speed (left column) and direction (right column) on 10 November 2007, for (a, b) Eyzonoi, (c, d) Axioupoli, (e, f) Akropotamos, and (g, h) Kymina. Verification measures are presented within the plots.

4.2. Model verification

For the verification of model performance, three statistical measures were computed: (a) the bias, (b) the root mean squared error (RMSE), and (c) the standard deviation of error (STDE). In addition, time series of observed and modeled wind speed and direction were constructed (Fig. 6). Observations and model data were paired adopting the nearest neighbor approach. In this frame, the model grid point nearest to the location of each measurement site was selected for extracting data used in the verification procedure.

It should be noted that for the circular variable of wind direction, the approach described in Carvalho et al. (2012) was used for calculating performance metrics. Among the above verification measures, STDE is thought to be of greater interest than RMSE and bias, due to the fact that it represents the dispersion of the model's error. In essence, a low STDE value indicates that the error is approximately constant and that model physics is correct, even if RMSE and bias exhibit large values. Conversely, a high STDE value indicates that the error is random and the model simulation lacks physical foundation, even if RMSE and bias show low values (Carvalho et al., 2012).

Overall, the WRF model showed good skill in terms of reproducing the evolution of the examined Vardaris event (Fig. 6). According to both observations and the numerical simulation, the episode initiated at around 0400–0600 UTC, as highlighted by the speed-up of wind and the turning toward a northwesterly (i.e. 315°) direction at all measurement sites. Wind speed was overestimated at the beginning of the event and underestimated toward the end, resulting to an underestimation of the duration of the event by approximately 2 h. Indeed, observations indicate the end of the event at around 1800–2000 UTC, whereas model results indicate the ending time at around 1600–1700 UTC. This could be attributed to the aforementioned tendency of WRF toward a faster than observed movement of the depression over southern Balkans (Section 4.1). Nevertheless, it is noticeable that the model was able to capture the peak intensity period of Vardaris quite successfully at all measurement sites, except at AXI for which an erroneous drop in wind speed was simulated (Fig. 6c).

The conducted verification procedure revealed low biases for wind speed, ranging from −0.06 m s^{-1} (EYZ; Fig. 6a) to 1.27 m s^{-1} (AXI; Fig. 6c). STDE values were found to be lower than 4 m s^{-1} at EYZ (Fig. 6a), AKR (Fig. 6e), and KYM (Fig. 6g), approximating 5 m s^{-1} at AXI (Fig. 6c). In terms of the wind direction, the computed biases range from 9.15° (EYZ; Fig. 6b) to 24.45° (AKR; Fig. 6f). Relatively large STDE values, exceeding 50°, were found for all measurement sites. However, much of this deviation can be attributed to discrepancies between observed and simulated direction before (0000–0355 UTC) and after (2005–2355 UTC) the Vardaris event. The above verification results suggest an overall satisfactory and consistent model performance, better than the one reported in the recent study of Tsopouridis et al. (2013) and comparable to past studies verifying NWP models for wind simulation (e.g. Carvalho et al., 2012; Deacu et al., 2010; Kotroni et al., 2014; Shimada et al., 2012).

Verification of the rest of the available parameters (Table 3), namely 2 m air temperature and vapor pressure, and mean sea-level pressure, enhanced the reliability of the numerical simulation, as also drawn from the examination of wind speed and direction. Low, negative biases were computed for air temperature, with STDE values approximating 2 °C at all measurement sites. Vapor pressure was also simulated successfully, showing STDE values lower than 1 hPa. With regards to sea-level pressure, it is evident that the WRF model underestimated this variable, with biases ranging from −0.36 hPa (EYZ) to −1.86 (KYM) and STDE values between 0.99 hPa (AKR) and 1.41 hPa (EYZ).

4.3. Analysis of the Vardaris episode

4.3.1. Near-surface wind flow

The spatiotemporal evolution of the near-surface flow during the course of the study day is presented in Fig. 7. Early in the morning at 0400 UTC, before the onset of strong wind flow, the approach of the depression's (Section 4.1) trailing cold front was clearly marked by the leading edge of the cold surge seen at the north-westernmost edge of the domain (Fig. 7a). Within the Axios Valley, the pressure gradient was weak, which resulted to light winds (<5 m s^{-1}) blowing from various directions.

Surface winds shifted to a north-northwesterly direction in the next 2 h, as the cold surge advanced into the study area. By 0600 UTC, strong northwesterly winds (>13–15 m s^{-1}) extended over the northernmost boundary of the valley, as shown in Fig. 7b. Along the valley, a pressure gradient of ~6 hPa was evident, with high pressures located north of Mt. Voras ("V1" and "V2") and low pressures to the south, over Mt. Paiko ("P"). This steep cross barrier pressure gradient allowed for the development of downslope flow (Koletsis et al., 2009a), significantly accelerating leeside winds downwind of Mt. Voras to above 18–20 m s^{-1}. Focusing on the east part of the valley, model results indicate that the onset of the Vardaris episode was marked by the generation of a gap outflow, as the wind was forced to pass through the narrow entrance of the valley in FYROM ("G"). On the west part of the valley, the flow was accelerated, with the downslope winds from Mt. Voras ("V2") possibly contributing to this intensification. Moreover, a flow splitting around Mt. Paiko resulted in a weak confluence on the lee of the barrier. Over the east edge of the domain, winds exhibited a deflection caused by the presence of Mt. Kroussia ("KR").

By 1200 UTC, the surge of cold air had penetrated in the study area (Fig. 7c). Winds significantly intensified across the entire domain, blowing predominantly from a northwestern direction. Storm winds (>28 m s^{-1}) developed downwind of Mts. Voras ("V3") and Kerkini ("K"), as a result of the downslope flow associated with the respective cross barrier pressure differences (~6 hPa for Mt. Voras and ~4 hPa for Mt. Kerkini). Along the Axios Valley, a wind shear line existed downwind of the Mt. Paiko ("P") creating an imaginary boundary zone (white box in Fig. 7c). Gale winds, exceeding 20 m s^{-1}, dominated at the east side of this zone, whereas to the west, the intensity of the flow was evidently lower (<15 m s^{-1}). This boundary zone (white box) was evidently the result of the interaction between the wind jet blowing over the east side of the valley, highlighting the main gap flow, and the downwind flow prevailing the west side, induced by Mt. Voras ("V3"). Evidently, the winds originating from the west side of the valley were forced to decelerate as they approached the jet, creating the boundary zone separating the two flows (e.g. Deacu et al., 2010).

At 1600 UTC, a remarkable weakening of the pressure gradient was evident (Fig. 7d), as the surface depression (Section 4.1) had began to move away from the study area (Fig. 5). This resulted to a significant reduction in the intensity of the Vardaris flow over the Axios Valley. Nevertheless, the influence of topography was still evident, with winds accelerating from ~5 to ~15 m s^{-1} as they moved through the narrow

Table 3
Summary of verification metrics for 2 m air temperature (AT) and vapor pressure (VP), and mean-sea pressure (MSL).

Variable	Bias				RMSE				STDE			
	EYZ	AXI	AKR	KYM	EYZ	AXI	AKR	KYM	EYZ	AXI	AKR	KYM
AT (°C)	−0.26	−1.13	−0.72	0.21	1.78	2.43	1.95	1.66	1.76	2.15	1.81	1.65
VP (hPa)	0.45	−1.75	0.52	0.59	0.83	1.92	0.88	1.09	0.69	0.79	0.72	0.92
MSL (hPa)	−0.36	−0.45	−1.26	−1.86	1.45	1.26	1.60	2.23	1.41	1.17	0.99	1.23

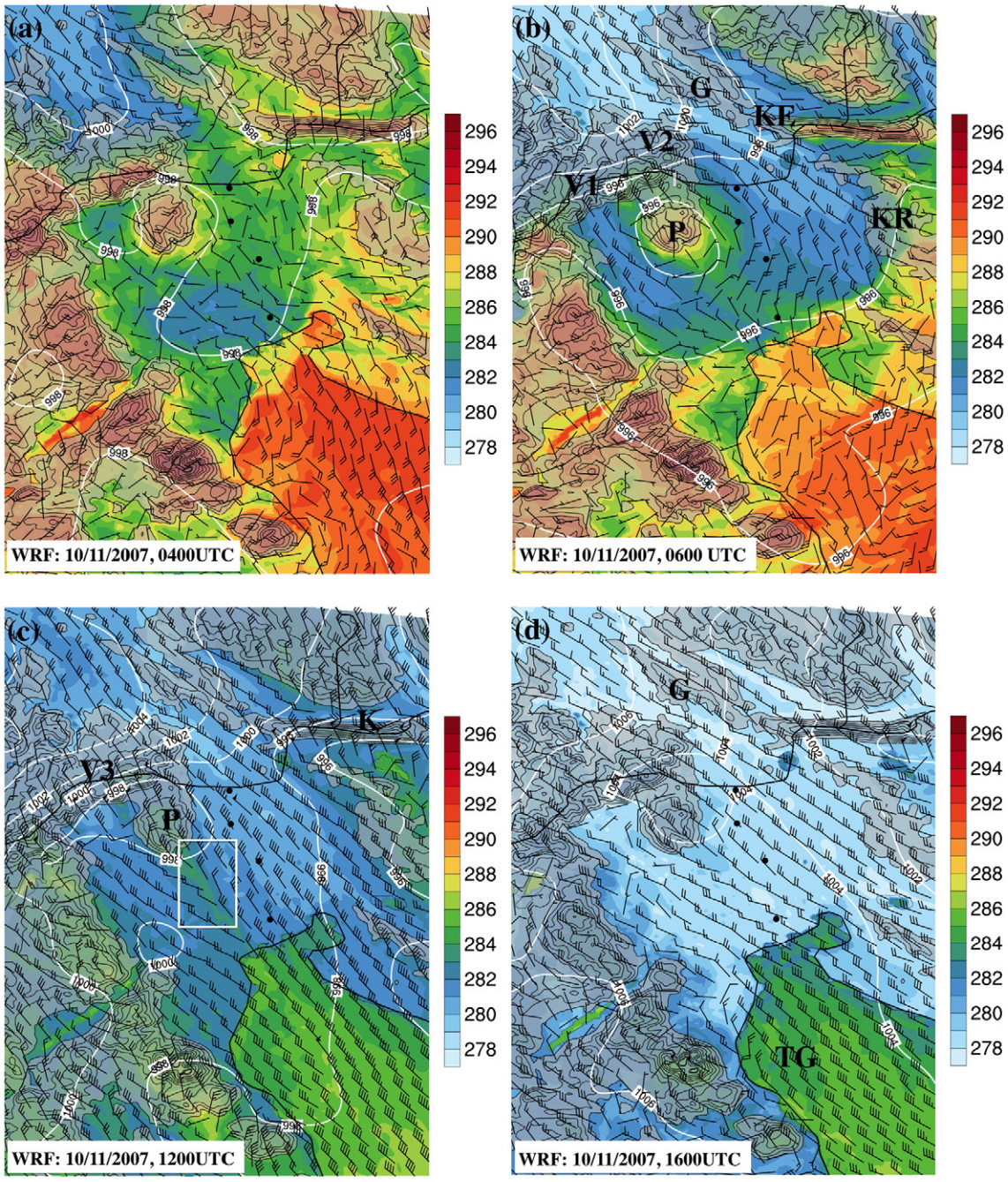

Fig. 7. Simulated 10 m wind barbs (full barb = 10 knots), 2 m potential temperature (shaded) and sea-level pressure (white contours at 2 hPa interval) on 10 November 2007 at (a) 0400 UTC, (b) 0600 UTC, (c) 1200 UTC, and (d) 1600 UTC. Regions where the model terrain exceeds 400 m are superimposed for reference (shaded light grey). Dots represent the locations of the measurement sites (refer also to Fig. 1b).

gap at the entrance of the valley in FYROM ("G"). Gale winds (>20 m s^{-1}) were only simulated over the Thermaikos Gulf ("TG"), as the northwesterly flow moved over the water and accelerated due to the decrease in frictional drag.

4.3.2. Upper-level wind flow

Investigation of the channeling effect of a valley requires, in principle, the study of ambient winds blowing above the valley (Whiteman and Doran, 1993; Carrera et al., 2009; Deacu et al., 2010). In the analysis that follows, the term "ambient winds" is used to refer to 800 hPa winds. This isobaric surface is typically found at a height of approximately 1800 m above mean sea level, which is generally higher than the mountains surrounding the Axios Valley (refer to Fig. 1b). Hence, the wind flow at this level is unlikely to be influenced by any channeling effect taking place within the valley. Looking at Fig. 8, one can easily notice that this key assumption is met, since an almost geostrophic flow of ambient winds was evident at all considered snapshots of the study day.

During the early stage of the event, ambient winds mostly had a cross-valley orientation (Figs. 8a, b). This clearly indicates that the large-scale flow could not have been simply diverted by the orographic barriers (i.e. forced channeling), or that there could have been a downward transfer of momentum, large enough to drive the flow within the valley. Therefore, neither can be considered as the dominant mechanism for the wind channeling taking place during the very first few hours of the Vardaris episode (Fig. 7b). Further examination of Fig. 8a

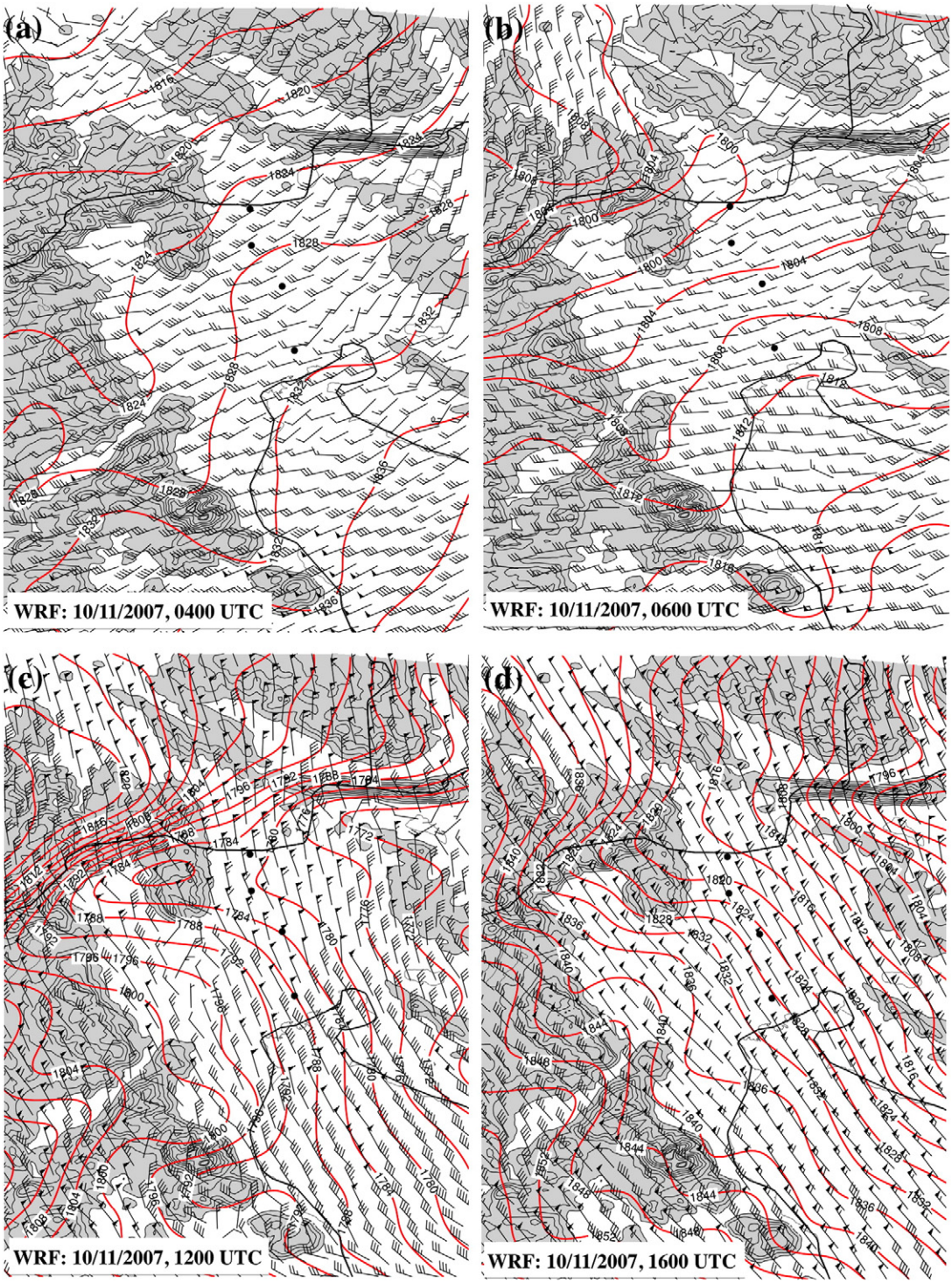

Fig. 8. Simulated 800 hPa wind barbs (full barb = 10 knots) and geopotential height (red contours at 4 m interval) on 10 November 2007 at (a) 0400 UTC, (b) 0600 UTC, (c) 1200 UTC, and (d) 1600 UTC. Regions where the model terrain exceeds 400 m are superimposed for reference (shaded light grey). Dots represent the locations of the measurement sites (refer also to Fig. 1b).

and b also reveals a thickening of the geopotential height contours, while retaining their cross-valley orientation. This suggests an increase in the along-valley component of the large-scale pressure gradient, which can be also seen in Figs. 7a and b. Considering the above, the mechanism of pressure-driven channeling (Whiteman and Doran, 1993) is thought to have played the major role in the development of the channeled wind during the initiation phase of the Vardaris episode. Thereafter, the contribution of forced channeling increased, as the above-valley flow shifted toward a northerly direction (Figs. 8c, d) and near-surface winds almost aligned with the valley's axis (Figs. 7c, d).

4.3.3. Vertical structure analysis

A cross-sectional analysis was conducted to elucidate the vertical structure of the flow during the considered Vardaris episode. The locations of the cross-sections, shown in Fig. 9, were selected so as to allow for a detailed study of the key features of the flow, which have

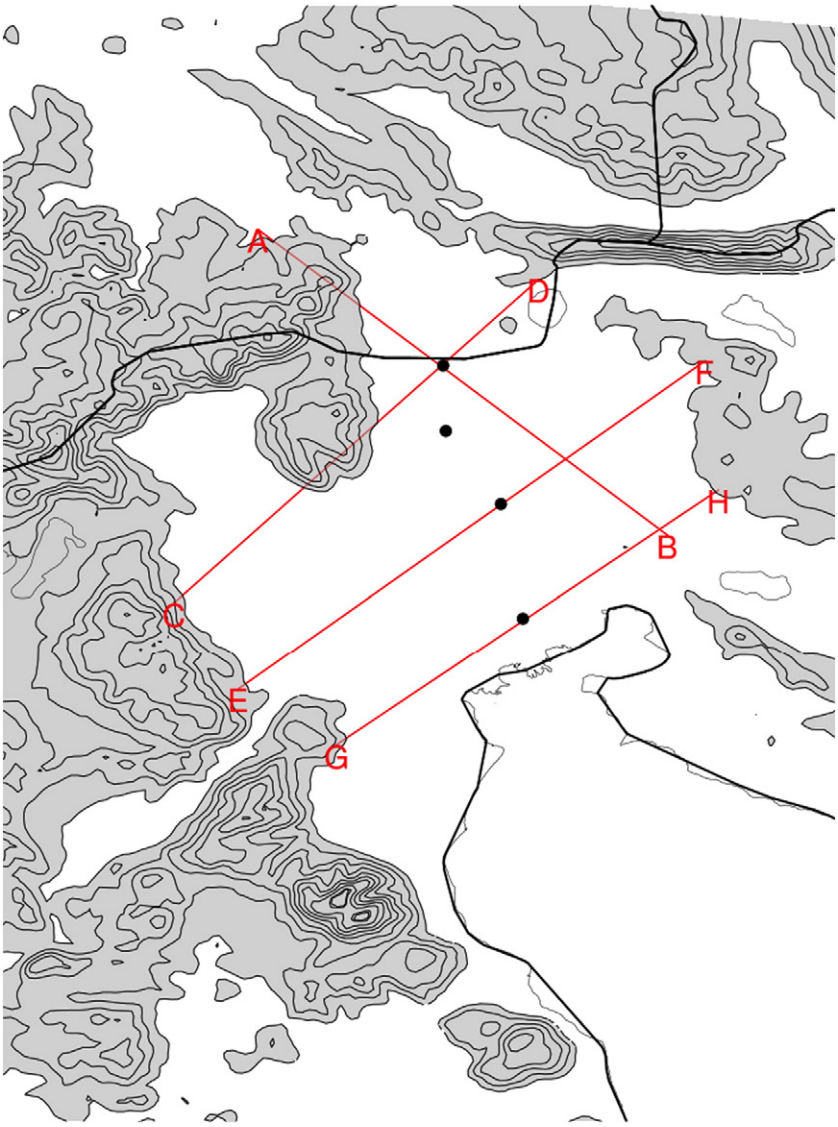

Fig. 9. Model-resolved topographic map of the study area (only regions with terrain elevation above 400 m are shown). Lines AB, CD, EF, and GH denote the positions of the cross-sections used for the respective analysis. Dots represent the locations of the measurement sites (refer also to Fig. 1b).

been previously highlighted (Section 4.3.1 and 4.3.2). The entire analysis was carried out for the initiation phase (10 November 2007, 0600 UTC), and for the period close the maximum of the event (10 November 2007, 1200 UTC).

Fig. 10a shows a northwest-southeast oriented cross-section of the meridional component of wind, which passes through the northernmost EYZ station and extends downstream (line AB in Fig. 9), valid at 10 November 2007 0600 UTC. During the initiation of the Vardaris episode, winds above the valley were predominantly blowing from southerly directions, whereas a northerly flow was evident at low levels and up to a height of approximately 1000–1500 m above sea level (asl). Behind Mt. Voras, close to the entrance of the valley in FYROM, northerly winds extended up to a height of 2700 m, indicating the approach of the Vardaris flow. Closer inspection of Fig. 10a reveals the occurrence of weak damming along the windward slopes of Mt. Voras, as evidenced by the isentropes tilting upward toward this orographic barrier. In addition, the generation of mountain waves was clearly evident at this stage of the event, as highlighted by the rapid downward and upward shifts of the isentropes, which were nearly parallel to the meridional wind contours. In essence, this particular vertical structure of the flow is considered to be typical of a downslope windstorm, with the mean critical level placed at ~2200 m asl over Mt. Voras and lowering downstream at ~1000 m asl over the valley. The upward vertically propagating mountain waves hit on this critical level and reflected their energy toward the surface, thus resulting in the amplification of the downslope winds. Such a structure of the lower troposphere is similar to the downslope windstorm configurations seen in other studies of wind flow with low critical levels (e.g. Durran and Klemp, 1987; Colle and Mass, 2000; Koletsis et al., 2009a).

Few hours later, at 1200 UTC, the penetration of the northwesterly flow further in the vertical dimension (Fig. 8c), resulted to the raise of the mean critical level at higher levels above Mt. Voras (~3500 m asl; Fig. 10b). Evidently, the strong northerly flow (>16 m s^{-1}) deepened and maximum wind speeds increased to above 25 m s^{-1}, merging into the gap flow. This is particularly highlighted by the presence of a layer of storm winds (>28 m s^{-1}) over the valley, extending from about 700 to 2000 m asl. A similar vertical structure was evident in the northwest-southeast oriented cross-section passing over the AXI station (not shown). Putting the above information together, it is evident that the strong winds over EYZ and AXI stations, where the

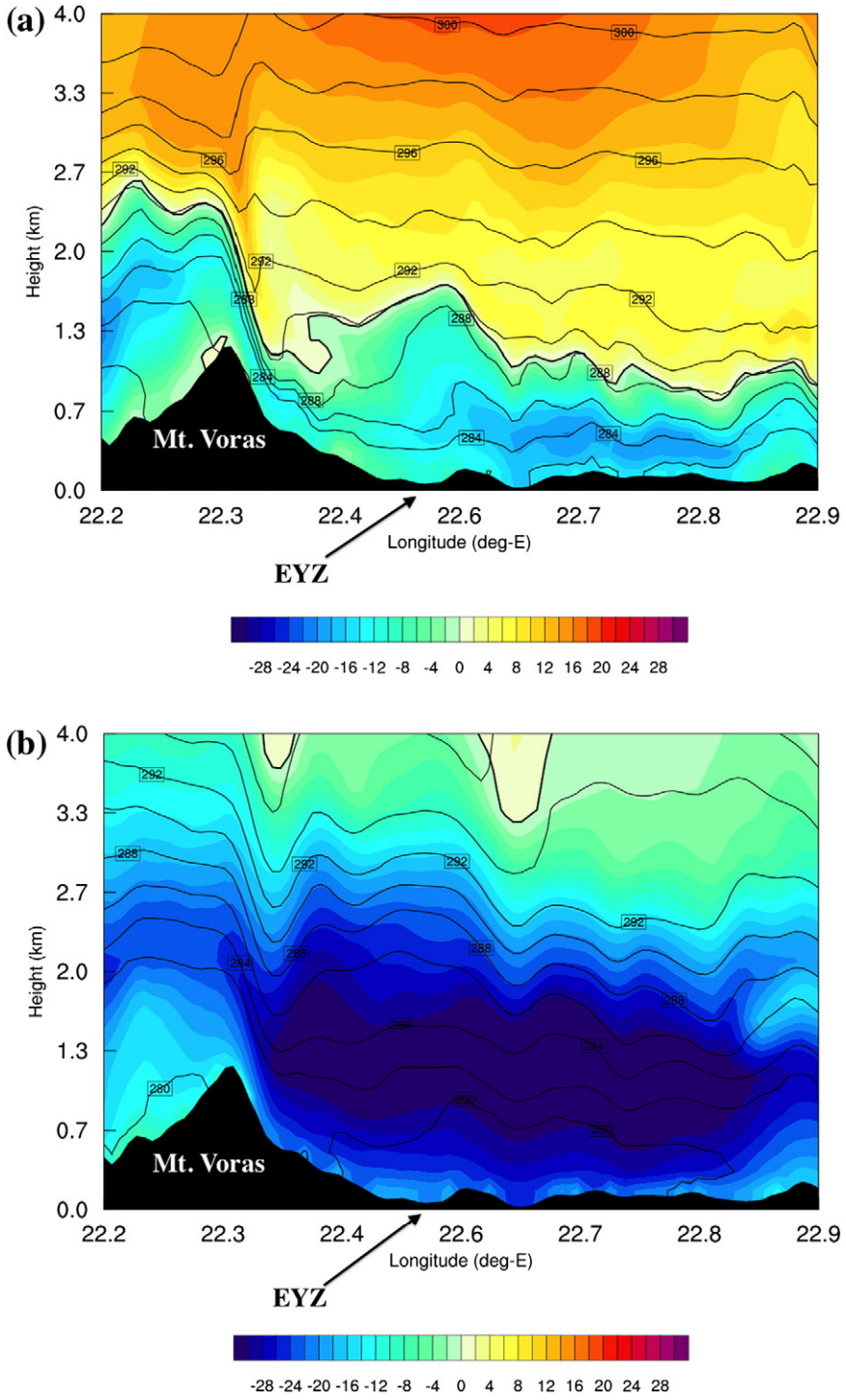

Fig. 10. Northwest to southeast vertical cross-section (line AB in Fig. 9) of the potential temperature (solid black lines at 2 K interval) and the meridional component of wind (shaded contours at 2 m s^{-1}), valid at (a) 0600 UTC and (b) 1200 UTC on 10 November 2007. The locations of Mt. Voras and EYZ station are marked on the plots.

maximum gust factors along the valley were also estimated (Section. 3.1), are most probably the result of the interaction between the downslope winds and the gap flow.

The cross-valley vertical structure of the atmosphere around the maximum of the Vardaris episode, on 10 November 2007 at 1200 UTC, is summarized in the cross-sections along lines CD, EF, and GH (Fig. 9), which are depicted in Fig. 11. Examination of the northernmost cross-section (line CD in Fig. 9) reveals the presence of an almost gap-parallel jet on the east side of the valley (Fig. 11a). This jet extended from the surface up to a height of ~2000 m asl, showing maximum wind speed values that exceeded 30 m s^{-1} in the layer between ~700 m asl and ~2000 m asl. Further, a shallow layer of cold air, portrayed by the area of low potential temperatures (<280 K) over the EYZ station, was evident, highlighting the penetration of the cold surge along the axis of the gap flow.

Further south, over the AKR station, the layer of storm winds was still evident in the lower troposphere, though its depth was clearly reduced (Fig. 11b). Over the KYM station, the depth of the jet was further restricted, extending from ~700 m asl up to ~1200 m asl, as the jet expanded over the gap exit (Fig. 11c). However, the most striking feature

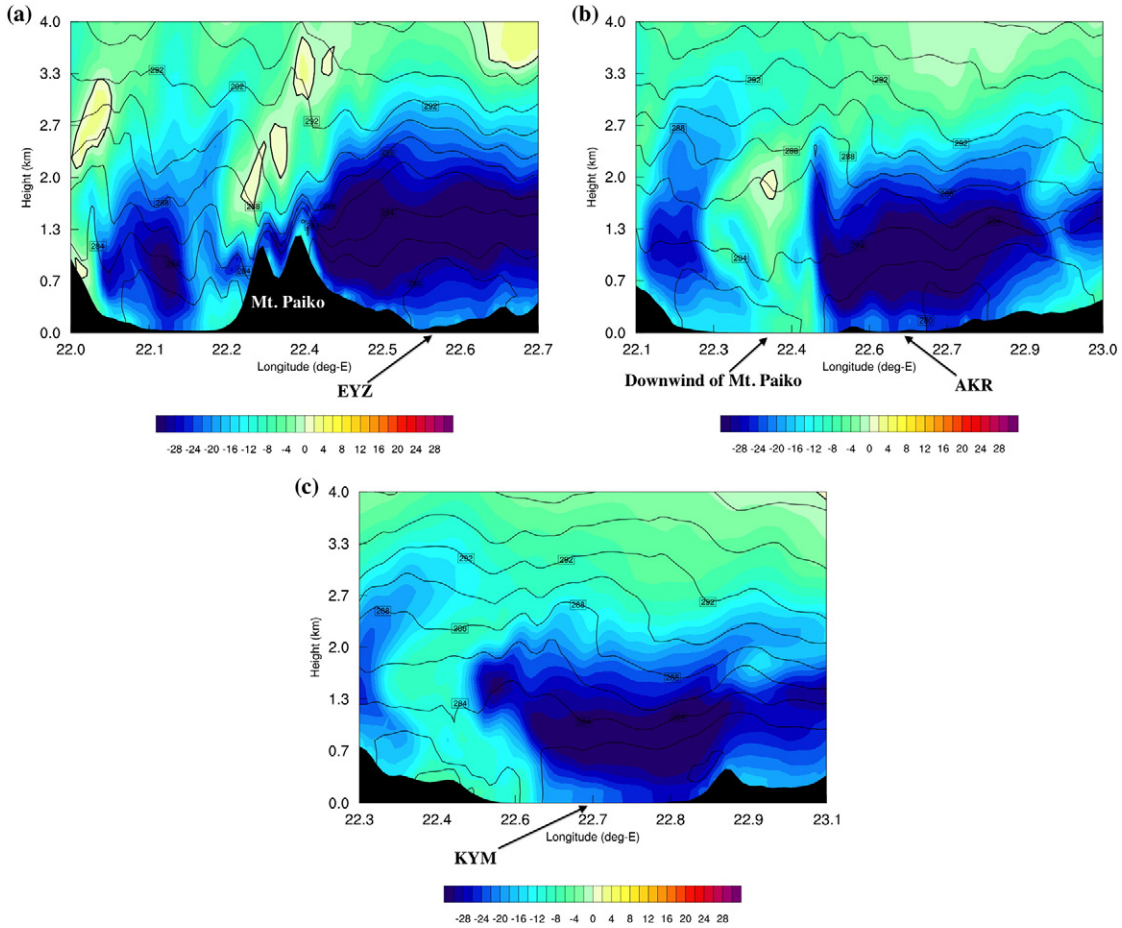

Fig. 11. Southwest to northeast vertical cross-section passing over (a) EYZ (line CD in Fig. 9), (b) AKR (line EF in Fig. 9), and (c) KYM (line IJ in Fig. 9) stations, of the potential temperature (solid black lines at 2 K interval) and the meridional component of wind (shaded contours at 2 m s^{-1}), valid at 1200 UTC on 10 November 2007. The locations of stations and key orographic features are denoted on the plots.

seen in Figs. 11b and c is the zone of relatively low winds downwind of Mt. Paiko. This wind shear line has been already discussed (Section 4.3.1) and is the result of the interaction between winds blowing on the west side of the valley with the barrier jet that developed on the east side of the valley.

5. Conclusions

Topography has been well documented as a key factor for the generation of dynamically and thermally driven local wind circulations. Vardaris, a northwesterly wind blowing in the Axios Valley in northern Greece, is considered to be a characteristic example of such topographically influenced wind regimes. It is well known for its consistent direction and high intensity, along with being an effective means for the advection of cold and dry air. Intense episodes of Vardaris are often associated with extensive damages in local infrastructures and agriculture.

In the current study, the characteristics of the Vardaris wind regime were first examined using observational data. The in situ measurements of wind and other meteorological variables were derived from a network of weather stations deployed within the Axios Valley during an 8-month period in year 2007. Analysis of these data confirmed previous studies (Angouridakis et al., 1981; Maheras et al., 1984; Psarri, 2005; Tsopouridis et al., 2013) in that Vardaris is the dominant regime in the study area, inducing near gale winds at all measurement sites and effectively advecting cold and dry air. Topography was found, based on a gust factor analysis, to play an important role in shaping the maximum intensity of wind. In particular, the two northernmost measurement sites exhibited the largest gust factor values, highlighting the impact of the surrounding complex orography in agreement with similar previous studies (e.g. Agustsson and Olafsson, 2004). Last, the analysis of the measured data provided indications for the association of the Vardaris wind flow with the occurrence of a gap flow along the Axios Valley.

At a second stage, numerical modeling was employed for examining the physical mechanisms responsible for the generation of an intense Vardaris episode. The numerical simulations were conducted with the state-of-the-art WRF model and were found to be in good agreement with observations. Analysis of the modeled data revealed that, considering the particular event, pressure-driven and forced channeling were the two dominant mechanisms for the occurrence of Vardaris. In particular, it was found that pressure-driven channeling played the key role during the initiation of the episode, while the importance of forced channeling increased toward the period of the maximum of the event. In accordance with the conclusions that were preliminary drawn from the analysis of the observational data, topography was found to significantly influence wind flow. Indeed, model results provided strong evidence for the occurrence of downslope windstorms along the orographic barriers at the northernmost edge of the Axios Valley, while a topographically induced wind shear line was also identified.

Overall, the results of the present study are considered to be a major contribution toward the better understanding of the important wind regime of Vardaris. To the authors' knowledge, the conclusions drawn from the analysis of both the observed and modeled data provide useful and previously unexplored insights to the physical mechanisms behind this particular wind flow. Nevertheless, it should be stressed out that our understanding for Vardaris could be further benefited by advancing

the present research, particularly in terms of expanding its observation to longer time periods and employing other sources of data (e.g. upper-air observations).

Acknowledgments

The present research has been financed by the "Development proposals of research entities-KRIPIS" framework, funded by N. P. "Competitiveness and Entrepreneurship," Action: THESPIA-Development of synergistic and integrated methods and tools for monitoring, management, and forecasting of environmental parameters and pressures. The European Center for Medium-range Weather Forecasts (ECMWF) is acknowledged for providing the analysis fields used in this study. Also, the authors would like to thank Department of Meteorology and Climatology (DMC) of the Aristotle University of Thessaloniki (AUTH), and especially Dr. Theodoros Karakostas and Dr. Ioannis Pytharoulis for their valuable contribution to the experiment.

References

Agustsson, H., Olafsson, H., 2004. Mean gust factors in complex terrain. Meteorol. Z. 13 (2), 149–155.
Angouridakis, V., Balafoutis, C., Maheras, P., 1981. Les vent de NW, et "Vardaris" a Thessalonique. Essai Statistique. Eaux et Climats. Melanges offert en homage a ChPEGUE, Grenoble (in French).
Borge, R., Alexandrov, V., del Vas, J.J., Lumbreras, J., Rodriguez, E., 2008. A comprehensive sensitivity analysis of the WRF model for air quality applications over the Iberian Peninsula. Atmos. Environ. 42 (8650-8574).
Carrera, M.L., Gyakum, J.R., Lin, C.A., 2009. Observational study of wind channeling within the St. Lawrence river valley. J. Appl. Meteorol. Climatol. 48, 2341–2361.
Carvalho, D., Rocha, A., Gomez-Gesteira, M., Santos, C., 2012. A sensitivity study of the WRF model in wind simulation for an area of high wind energy. Environ. Model. Softw. 33, 23–34.
Challa, V.S., Indracanti, J., Rabarison, M.K., Patrick, C., Baham, J.M., Young, J., Hughes, R., Hardy, M.G., Swanier, S.J., Yerramilli, A., 2009. A simulation study of mesoscale coastal circulations in Mississippi Gulf coast. Atmos. Res. 91, 9–25.
Cogliati, M., Mazzeo, N.A., 2006. Air flow analysis in the upper Rio Negro Valley (Argentina). Atmos. Res. 80, 263–279.
Colle, B.A., Mass, C.F., 1998. Windstorms along the western side of the Washington Cascade Mountains. Part I: A high-resolution observational and modeling study of the 12 February 1995 Event. Mon. Wea. Rev. 126, 28–52.
Colle, B.A., Mass, C.F., 2000. High-resolution observations and numerical simulations of easterly gap flow through the Strait of Juan de Fuca on 9–10 December 1995. Mon. Weather Rev. 128, 2398–2422.
Czyzyk, S., Bell, C., 2007. Forecast challenges and impacts of severe downslope wind events. Proceedings of the 22nd Conference on Weather Analysis and Forecasting/18th Conference on Numerical Weather Prediction, pp. 25–29 (June, Park Ceity, UT, USA).
Deacu, D., Zadra, A., Hanesiak, J., 2010. Simulating wind channeling over Frobisher Bay and its interaction with downslope winds during the 7–8 November 2006 wind event. Atmosphere-Ocean 48 (2), 101–121.
Durran, D.R., 1990. Mountain waves and downslope winds. Meteorol. Monogr. 23, 59–81.
Durran, D.R., Klemp, J.B., 1987. Another look at downslope winds. Part II: Nonlinear amplification beneath wave-overturning layers. J.Atmos.Sci. 44, 3402–3412.
Eckman, R.M., 1998. Observations and numerical simulations of winds within a broad forested valley. J. Appl. Meteorol. 37, 206–219.
Esau, I., Repina, I., 2012. Wind climate in Kongsfjorden, Svalbard, and attribution of leading wind driving mechanisms through turbulence-resolving simulations. Adv. Meteorol., 568454
Giannoulakis, I., 2014. Synoptic and Dynamic Study of Snowfall in Thessaloniki. M.Sc. Thesis, Aristotle University of Thessaloniki, Thessaloniki, Greece, p. 114 (in Greek).
Gross, G., Wippermann, F., 1987. Channeling and counter-current in the upper Rhine Valley: numerical simulations. J. Clim. Appl. Meteorol. 26, 1293–1304.
Iacono, M.J., Delamere, J.S., Mlawer, E.J., Shephard, M.W., Clough, S.A., Collins, W.D., 2008. Radiative forcing by long–lived greenhouse gases: calculations with the AER radiative transfer models. J. Geophys. Res. 113, D13103.
Janjic, Z.I., 1994. The step-mountain eta coordinate model: further developments of the convection, viscous sublayer and turbulence closure schemes. Mon. Weather Rev. 122, 927–945.
Jarvis, A., Reuter, H.I., Nelson, A., Guevara, E., 2008. Hole-filled SRTM for the globe Version 4, available from the CGIAR-CSI SRTM 90m Database. http://srtm.csi.cgiar.org.
Kain, John S., 2004. The kain–fritsch convective parameterization: an update. J. Appl. Meteor. 43, 170–181. http://dx.doi.org/10.1175/1520-0450(2004)0432.0.CO;2.
Koletsis, I., Lagouvardos, K., Kotroni, V., Bartzokas, A., 2009b. The interaction of northern wind flow with the complex topography of Crete Island – part 1: observational study. Nat. Hazards Earth Syst. Sci. 9, 1845–1855.
Koletsis, I., Lagouvardos, K., Kotroni, V., Bartzokas, A., 2009a. Numerical study of a downslope windstorm in northwestern Greece. Atmos. Res. 94, 178–193.
Koletsis, I., Lagouvardos, K., Kotroni, V., Bartzokas, A., 2010. The interaction of northern wind flow with the complex topography of Crete Island – part 2: numerical study. Nat. Hazards Earth Syst. Sci. 10, 1115–1127.
Kossmann, M., Sturman, A.P., 2003. Pressure-driven channeling effects in bent valleys. J. Appl. Meteorol. 42, 151–158.
Kotroni, V., Lagouvardos, K., Lykoudis, S., 2014. High-resolution model-based wind atlas for Greece. Ren. Sust. Energ. Rev. 30, 479–489.
Lackmann, G.M., Overland, J.E., 1989. Atmospheric structure and momentum balance during a gap-wind event in the Shelikof Strait. Alaska. Mon. Wea. Rev. 117, 1817–1833.
Lennard, C., 2014. Simulating an extreme wind event in a topographically complex region. Bound.-Layer Meteorol. 153, 237–250.
Maheras, P., Flocas, A., Karacostas, T., 1984. La structure de la basse troposphere pendant le vent Vardaris a Thessalonique. Zbornik 10, 241–243 (in French).
Manor, A., Berkovic, S., 2015. Bayesian Inference aided analog downscaling for near-surface winds in complex terrain. Atmos. Res. 27–36 164-165.
Mayr, G.J., Armi, L., Gohm, A., Zangl, G., Durran, D.R., Flamant, C., Gabersek, S., Mobbs, S., Ross, A., Weissmann, M., 2007. Gap flows: results from the Mesoscale Alpine Programme. Q. J. R. Meteorol. Soc. 133, 881–896.
Miglietta, M.M., Zecchetto, S., De Biasio, F., 2013. A comparison of WRF model simulations with SAR Wind data in two case studies of orographic lee waves over the Eastern Mediterranean Sea. Atmos. Res. 120, 127–146.
Overland, J.E., Walter, B.A., 1981. Gap winds in the Strait of Juan de Fuca. Mon. Weather Rev. 109, 2221–2233.
Papanastasiou, D.K., Melas, D., Lissaridis, I., 2010. Study of wind field under sea breeze conditions; an application of WRF model. Atmos. Res. 98, 102–117.
Psarri, L., 2005. The Local Wind of Thessaloniki, Vardaris – An Approach to the Problem with Classical Methods and the Use of Artificial Neural Networks. M.Sc. Thesis. Aristotle University of Thessaloniki, Thessaloniki, Greece (in Greek).
Puliafito, S.E., Allende, D.G., Mulena, C.G., Cremades, P., Lakkis, S.G., 2015. Evaluation of the WRF model configuration for Zonda wind events in a complex terrain. Atmos. Res. 166, 24–32.
Reed, T.R., 1931. Gap winds of the Strait of Juan de Fuca. Mon. Weather Rev. 59, 373–376.
Reid, S., 1996. Pressure gradients and winds in Cook Strait. Weather Forecast. 11, 476–488.
Santos-Alamillos, F.J., Pozo-Vázquez, D., Ruiz-Arias, J.A., Tovar-Pescador, J., 2015. Influence of land-use misrepresentation on the accuracy of WRF wind estimates: evaluation of GLCC and CORINE land-use maps in southern Spain. Atmos. Res. 157, 17–28.
Sharp, J., Mass, C.F., 2004. Columbia Gorge gap winds: their climatological influence and synoptic evolution. Weather Forecast. 19, 970–992.
Shimada, T., Sawada, M., Sha, W., 2012. Low-level easterly winds blowing through the Tsugaru Strait, Japan. Part II: numerical simulations of the event on 5–10 June 2003. Mon. Weather Rev. 140, 1779–1793.
Simon, A., Kank, J., Sokol, A., Putsay, M., Uhrinova, L., Csirmaz, K., Okon, L., Habrovsky, R., 2011. Case study of a severe windstorm over Slovakia and Hungary on 25 June 2008. Atmos. Res. 100 (4), 705–739.
Skamarock, W.C., Klemp, J.B., Dudhia, J., Gill, D.O., Barker, D.M., Duda, M.G., Huang, X.Y., Wang, W., Powers, J.G., 2008. A description of the Advanced Research WRF version 3. NCAR Technical Note, NCAR/TN-475 + STR, Mesoscale and Microscale Meteorology Division. National Centre for Atmospheric Research, Boulder, Colorado, USA.
Steenburgh, W.J., Schultz, D.M., Colle, B.A., 1998. The structure and evolution of gap outflow over the Gulf of Tehuantepec. Mexico. Mon. Wea. Rev. 126, 2673–2691.
Tewari, M., Chen, F., Wang, W., Dudhia, J., LeMone, M.A., Mitchell, K., Ek, M., Gayno, G., Wegiel, J., Cuenca, R.H., 2004. Implementation and verification of the unified NOAH land surface model in the WRF model. Proceedings of the "20th Conference on Weather Analysis and Forecasting/16th Conference on Numerical Weather Prediction", pp. 11–15.
Thompson, G., Field, P.R., Rasmussen, R.M., Hall, W.D., 2008. Explicit forecasts of winter precipitation using an improved bulk microphysics scheme. Part II: implementation of a new snow parameterization. Mon. Weather Rev. 136, 5095–5115.
Tsopouridis, L., Pytharoulis, I., Karacostas, T., Zanis, P., Tegoulias, I., 2013. Numerical study of an intense episode of Vardaris wind. In: Helmis, C.G., Nastos, P.T. (Eds.), Advances in Meteorology, Climatology and Atmospheric Physics, pp. 325–332.
Weber, R.O., Kaufmann, P., 1998. Relationship of synoptic winds and complex terrain flows during the MISTRAL field experiment. J. Appl. Meteorol. 37, 1486–1496.
Whiteman, D.C., Doran, J.C., 1993. The relationship between overlying synoptic-scale flows and winds within a valley. J. Appl. Meteorol. 32 (1669-1682), 1993.
World Meteorological Organization, 2000. General Meteorological Standards and Recommended Practices, Appendix A, WMO Technical Regulations, WMO-No. p. 49.